Journal of Alloys and Compounds 851 (2021) 156924

Contents lists available at ScienceDirect

Journal of Alloys and Compounds

journal homepage: http://www.elsevier.com/locate/jalcom

Experimental observation of two-stage crystallization of $Ge_2Sb_2Te_5$ amorphous thin films under the influence of a pulsed laser

Tatyana Kunkel [a, *], Yuri Vorobyov [c], Mikhail Smayev [d, e], Petr Lazarenko [f], Vladimir Veretennikov [f], Vladimir Sigaev [d], Sergey Kozyukhin [b]

[a] Moscow Institute of Physics and Technology, 9 Institutskiy Per., Dolgoprudny, 141701, Russia
[b] Kurnakov Institute of General and Inorganic Chemistry, Russian Academy of Sciences, 31 Leninski Pr., Moscow, 119991, Russia
[c] Ryazan State Radio Engineering University, 59/1 Gagarin St., Ryazan, 390005, Russia
[d] Mendeleev University of Chemical Technology of Russia, 9 Miusskaya Sq., Moscow, 125047, Russia
[e] Lebedev Physical Institute, Russian Academy of Sciences, 53 Leninsky Pr., Moscow, 119991, Russia
[f] National Research University of Electronic Technology, 1 Shokin Sq., Zelenograd, 124498, Russia

ARTICLE INFO

Article history:
Received 18 June 2020
Received in revised form
20 August 2020
Accepted 26 August 2020
Available online 28 August 2020

Keywords:
$Ge_2Sb_2Te_5$
Phase-change materials
Thin films
Femtosecond laser
Crystallization
Atomic force microscopy

ABSTRACT

The nature of crystallization in telluride based phase change memory materials is being actively discussed, and we present new experimental results on the effect of a pulsed laser treatment on the amorphous thin film crystallization of composition $Ge_2Sb_2Te_5$ (GST225). It is shown that there are two ways of crystalline phase formation under femtosecond pulses excitation. At the moderate value of laser fluence, crystalline fraction forms inside the solid amorphous phase. This process is apparently two-stage, and this leads to formation of fine-grained polycrystalline material. The second way of crystallization proceeds at higher levels of the laser fluence, closer to the beam axis. In this case, larger grains are produced closer to the beam axis, and eventually no new nuclei can be formed due to high cooling velocity leading to inhibition of nucleation. The article also presents the results on the effect of the substrate type (metallic or oxide) and film thickness on crystallization, which is due to the light penetration depth and reflection from the film-substrate interface.

1. Introduction

Crystallization is one of the key problems for telluride based phase change memory (PCM) materials, and a large number of both experimental and theoretical works have dealt with this phenomenon since the discovery by Yamada and coauthors of fast switching stable compositions on the pseudo-binary line between GeTe and Sb_2Te_3 (GST alloys) [1–9]. The majority of studies were performed for amorphous PCM thin films; substantially fewer studies were conducted for nanosize objects [10–13]. But the paradox is that there are practically no studies in which separation into surface and bulk crystallization is carried out, which, from our point of view, does not give a complete picture of the crystallization of amorphous PCM thin films.

Studies of surface crystallization during the “amorphous - crystalline” phase transition attract sufficient attention since this provides important information about the kinetics of the process, and also about the crystallization mechanism as a whole in the material. In addition, there are surface processes that initiate this bulk phase transition. For example, bulk phase transitions of cesium hydrogen sulphate can be controlled by modifying the water vapour pressure above the salt, i.e. a surface process triggers phase transitions in the bulk [14]. Laser treatment is a common way to initiate surface crystallization, and the pulsed lasers attract special attention since in this case not only the wavelength can be varied, but also such parameters as the pulse duration, repetition rate, and number of pulses. Nonlinear effects are also possible and this area has been scantily studied for PCM materials. It should be noted that these phenomena for chalcogenide vitreous semiconductors are well studied; for example, see Ref. [15] and literature therein.

The problem is that if we study nanosize thin films and want to separate surface and bulk crystallization, the question arises of how to perform this experimentally. A similar question arises in the case of experimental phase transition study of any nanoscale objects. It is necessary to find experimental methods that would be connected in a certain way either with the surface or with the bulk (even if we

* Corresponding author. IGIC RAS, 31 Leninski Pr., Moscow, 119991, Russia.
E-mail address: tatanakunkel@gmail.com (T. Kunkel).

https://doi.org/10.1016/j.jallcom.2020.156924
0925-8388/

are considering a thin film), and in doing so they would predictably react to phase transitions. A possible way to solve this problem is to use two types of experimental methods: some investigate surface states, others investigate bulk, and then identify the correlations of the results. A similar algorithm was used to study so-called solid water, for example; as a result, the authors obtained information about surface and bulk or "top-down" crystallization [16].

The basic property of GST materials is that they can be prepared in an amorphous state only either as a thin film on a substrate or as nanoparticles, but herein bulk amorphous material cannot be prepared. Accordingly, the aspect of surface crystallization for GST amorphous thin films must be considered anyway. The use of a pulsed laser as an external action initiating a phase transition prevail over several advantages in this regard. Firstly, the light penetration depth will be different at various laser wavelengths since the optical absorption coefficient varies. We can consider a layer in which strong electronic excitation and subsequent electron-phonon relaxation will take place, and a layer into which heat penetrates due to the thermal conductivity of the material. The latter process has a diffusion nature, and it corresponds to bulk crystallization to a large extent. Secondly, we can change the film thickness and the type of substrate materials (dielectric or conductive) and, accordingly, reveal the effect of these parameters on the crystallization of the as-deposited amorphous film with varying exposure parameters.

Thus, in this study, we investigated the mechanisms of crystalline marks formation on the surface of amorphous GST225 thin films upon a femtosecond multi-pulsed laser irradiation using experimental methods that provide information primarily on surface processes. Such methods include optical microscopy and atomic-force microscopy (AFM).

2. Methods

2.1. Sample preparation and thin film characterization

Thin films (30, 80 and 130 nm) of $Ge_2Sb_2Te_5$ composition (GST225) were deposited on two different substrate types to study the influence of contacting layers on the process of laser-induced modification. First, thermally oxidized Si substrates (oxide thickness is about 1 μm), and, second, the same oxidized substrates with W (200 nm)/TiN (50 nm) metallic layers on the top of them were used. The tungsten layer was used as a contact layer for the GST225 thin film. The main role of the TiN layer was to serve as an adhesion sublayer for the tungsten. Below we refer to them simply as *dielectric* and *conductive* for brevity. A *dc* magnetron sputtering of the polycrystalline target was employed for GST225 deposition.

The residual pressure in the chamber before the deposition was $3.0 \cdot 10^{-3}$ Pa, the pressure of Ar during the process was $5.7 \cdot 10^{-1}$ Pa, and the dc power was 25 W. Elemental composition of the films was determined by the time-of-flight secondary ion mass spectrometer (IonTOF TOF. SIMS 5) together with the Auger spectroscopy (PerkinElmer PHI-660). The composition of the films was close to $Ge_2Sb_2Te_5$, the elemental distribution was uniform across the film thickness. The structure of the GST films was studied by X-ray diffraction (XRD, Rigaku SmartLab). According to the XRD data, the as-deposited films were amorphous.

2.2. Laser irradiation

The setup scheme used for laser modification of GST films is shown in Fig. 1(a). We use a Yb:KGW laser system (Light Conversion Pharos SP) with a regenerative amplifier operating at a wavelength of 1030 nm. The pulse duration value of 185 fs was determined with the autocorrelator (APE pulseCheck). The repetition rate of laser

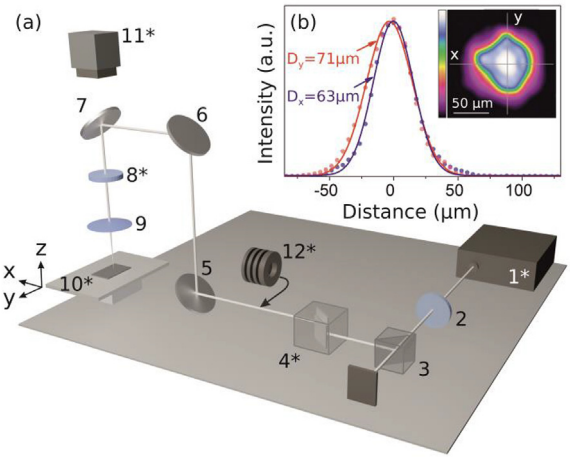

Fig. 1. (a) Scheme of the experimental setup for femtosecond modification of the GST films: *1* - Yb:KGW laser system (λ = 1030 nm), *2* - half-wave plate, *3* - polarizing beam splitting cube, *4* -attenuator, *5, 6, 7* - mirrors, *8* - motorized half-wave plate, *9* - lens, *10* - GST sample on the XYZ-motorized stage, (*11*) CCD camera, *12* - laser power meter with thermopile sensor. Asterisks next to numbers mean computer control. (b) The intensity distribution map of laser beam (on the inset) and corresponding Gaussian-shaped profiles of intensity along X and Y axes.

pulses could be changed in the range of 1 kHz ÷ 1 MHz. Motorized attenuator (Altechna Watt Pilot) was employed to control the energy of the pulse. The GST films were housed on the translational air-bearing stage (Aerotech ABL1000) that allows the programmable positioning of the samples providing an opportunity to perform multiple excitations in a reasonable amount of time. The normally incident light beam was focused on the sample surface with a 75-mm focal length lens (Thorlabs LA1608-B). The beam diameter on the GST surface was measured with a CCD camera profiler (Ophir Spiricon SP620U) and was about 70 μm (Fig. 1 b). The beam polarization was linear and its direction was controlled using a motorized half-wave plate. The process of laser modification was visualized with a CCD color camera (QImaging Retiga 3000) and white light source (Thorlabs OSL2 Fiber Light Illuminator).

During the laser irradiation experiments we recorded one and the same array of marks in all GST samples under study. Pulse energy was changed from 50 nJ to 2 μJ. The number of pulses delivered to the single mark varied from 1 up to 2^{20} (1, 2, 4, 8, etc.).

The laser wavelength 1030 nm (1.2 eV) corresponds to the absorption coefficient $\alpha \sim 1 \times 10^5$ cm^{-1} for GST [17], and light penetration depth is $1/\alpha$ of about 100 nm. The photon energy at the wavelength of irradiation is larger than the amorphous GST bandgap 0.7 eV [17].

2.3. Characterization techniques

Crystallization of GST is accompanied by an increase in the material density and an increase in conductivity. Furthermore, during crystallization a characteristic grain microstructure forms inside the material. Itself being extremely sensitive to the surface properties, the atomic-force microscopy (AFM) allows to detect such changes with nanoscale resolution without long sample preparation. The AFM measurements were performed on an NTEGRA Aura AFM (NT-MDT). The HA_C/W2C + cantilevers (NT-MDT) with W_2C conductive coating, a tip radius <35 nm and resonant frequency of 17.8 kHz (stiffness about 0.26 N/m) were used. The tapping mode topography mapping for registration of density changes was carried out with free/set point oscillation amplitude of about 10 nm/7 nm. The mapping of spreading current signal was

measured in contact mode with pressing force of the probe to the sample of about 1.5 nN. The bias voltage at the probe with respect to the grounded substrate was −4 V. All measurements were carried out in ambient conditions.

Micro-Raman measurements were performed using the NTEGRA Spectra Setup (NT-MDT) with the aim to identify the phase state of the material. A 532 nm laser was utilized; the power was limited to 0.5 mW to avoid any laser-induced changes in the GST during continuous exposure. Spectra were obtained using 1800 mm^{-1} diffraction grating. Accumulation of a spectrum took 150 s to provide a reasonable signal-to-noise ratio.

3. Results

Bright field optical images of laser induced marks are shown in Fig. 2. These particular images were obtained for the 30 nm film on the conductive substrate and these are typical for our study. The tendency of area growth with increased number of pulses is readily observed. For pulse energy less than 100 nJ no modification was observed even for one million of laser pulses. Higher energies lead to bright marks formation. Under excitation with less than 128 pulses, however, only pale spots could be seen; the optical contrast with the surroundings is less than 5% there. For low pulse energies (e.g. 100 nJ in Fig. 2), the modification becomes observed only after a considerable number of pulses. In contrast, higher values of energy lead to formation of the pale spots even under a single-pulse excitation (see left column in Fig. 2). We must note that the possibility of modification, at least the visible one, of GST surface with a single ultra-short (either femto- or picosecond) laser pulse is not widely established in the literature. Single femtosecond pulse crystallization is reported in Refs. [18], and the reverse process, amorphization of crystalline material, is demonstrated in Refs. [19]. Conversely, the authors of [20] claimed that in their study neither crystallization of amorphous material nor amorphization of crystalline one were achieved using a single-pulse excitation. Our results indicate that there is at least the pulse energy threshold to achieve the modification of as-deposited amorphous film. The detailed nature of this modification will be addressed below.

The last thing worth mentioning at this stage is that, despite the images in Fig. 2 were obtained for the specific sample, other samples exhibit the similar behavior of the modified areas formation. Moreover, we have tested a variety of pulse repetition rates ranging from 1 kHz up to 1 MHz with constant pulse energy and no differences were observed, neither in the area of bright spots nor their overall appearance. All the results we report in this study correspond to the 200 kHz repetition rate.

In Fig. 3 the results of recorded mark characterization using AFM together with the optical methods are demonstrated. The bright spot forms under the influence of repetitive laser pulses. Crystallization of GST is known to increase its reflectivity justifying its use in optical information storage. Further evidence of the laser-induced phase transition is provided by AFM. Firstly, it shows that the surface of the bright spot is lower than surrounding initial material, which is in line with the density change of GST upon crystallization [21,22]. Secondly, the conductive AFM shows the greater value of electrical current through the transformed region, which conforms with the crystallization of GST as well. The rippled area at the edge of the bright spot is a characteristic feature of ultrashort laser influence on GST; further details could be found in Ref. [23]. Raman spectra show the redshift of the main spectral band upon laser-induced transition, which is also a feature of crystallization [24]. All things considered, the bright areas formed as a result of laser excitation are undoubtedly crystalline.

As it can be seen from Figs. 2 and 3, the boundaries of the regions corresponding to different phases are quite sharp. An increase of the laser pulse energy leads to an increase of the crystal spot size (bottom to top in Fig. 2). These observations can be explained by taking into account the uneven distribution of the intensity in the laser beam. We assume that the modification occurs only in the region where the laser fluence reaches a certain level — threshold fluence of crystallization (TFC). The notion of TFC is illustrated in Fig. 4 (a); diameters of crystallized regions together with the laser beam profile (Fig. 1 b) allow the determination of TFC value. We have estimated the effect of laser parameters (such as number of pulses and pulse energy), substrate type and film thickness on the level of TFC.

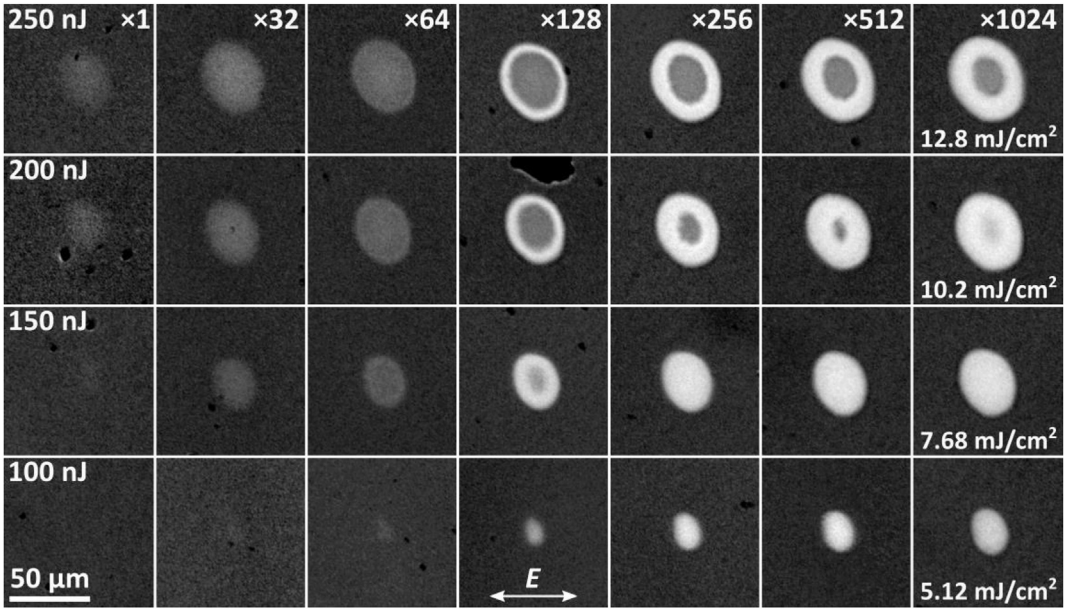

Fig. 2. Optical images (with optimized contrast) of the laser-induced marks recorded on the 30 nm GST film on the conductive substrate. Pulse energy, maximum fluence and number of laser pulses are denoted. Double-headed arrow shows the polarization of the laser beam.

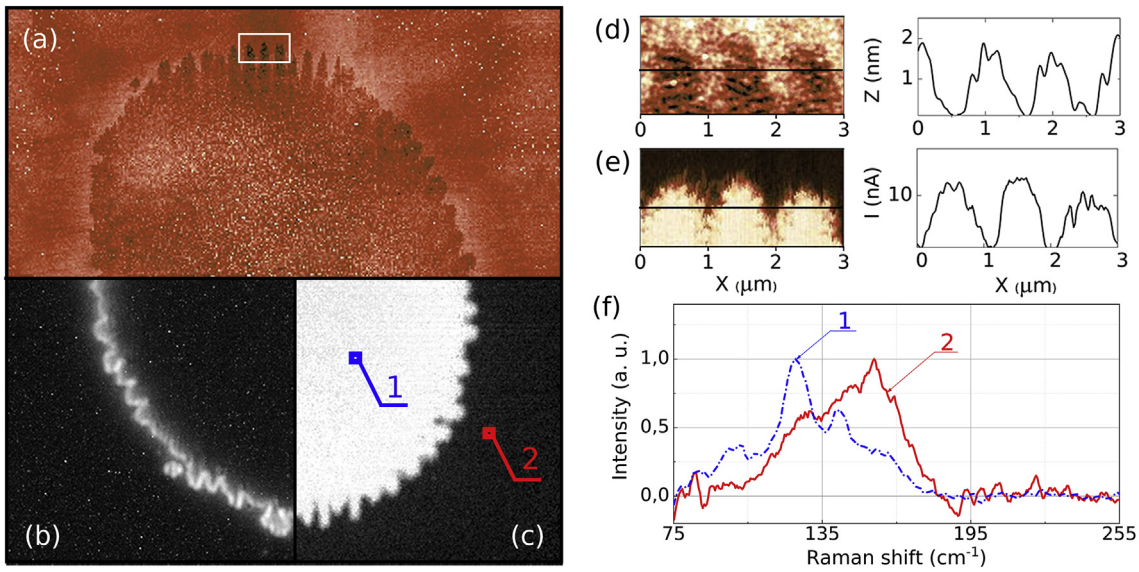

Fig. 3. Characterization of a recorded mark (200 nJ, × 2^{15} pulses, 80 nm-thick GST layer on the conductive substrate) using AFM, optical microscopy and Raman spectroscopy. Tapping-mode AFM image (a), dark-field (b) and bright-field (c) optical images of the same mark are overlaid; image size is 42 × 42 μm^2. AFM topography and its profile are presented in (d) for the small region outlined in (a); the corresponding current map and its profile are shown in part (e). The panel (f) shows normalized Raman spectra obtained from points 1 and 2 defined in image (c).

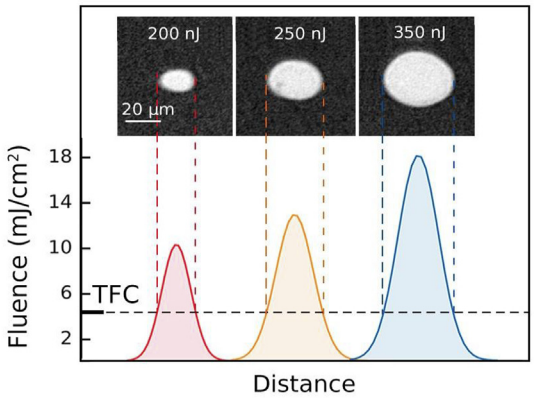

Fig. 4. TFC determination on the fluence profile by the diameter of the corresponding crystallized spot and its independence from the pulse energy. The maximum fluences, at which spots were formed, are shown on optical images.

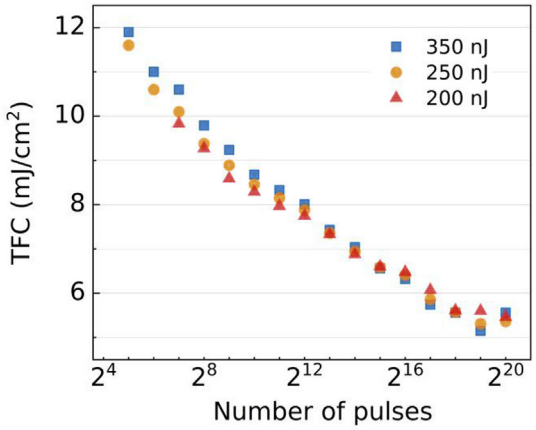

Fig. 5. TFC dependence on the laser pulse repetitions count for different values of pulse energy, obtained for the sample with 80 nm GST film on the dielectric substrate.

Fig. 5 shows that the TFC depends strongly on the number of laser pulses hitting the sample. The value of pulse energy practically does not affect the TFC for a given film thickness, and type of substrate. The relative scatter of TFC values obtained for different pulse energies is below 5% for any number of laser pulses and could be attributed to the uncertainty of measurement.

Absence of TFC dependence on the pulse energy suggests that the *local* laser fluence solely controls the formation of crystalline fraction, at least in the outer area of laser-induced marks, which was used for the TFC determination. In Fig. 4, such TFC level is denoted on the fluence profiles that leads to the formation of crystalline spots of certain diameters under pulses of different energy. Another implication which could be drawn from this conclusion is that lateral heat flow does not participate significantly in the process of marks formation. Indeed, according to the published data [21,25] the thermal diffusivity of GST could be estimated as $1.6 \cdot 10^{-7}$ m^{2}s^{-1}, which even for the longest characteristic time in our experiment (pulses period 5 μs) corresponds to the characteristic distance of heat diffusion of less than 2 μm. First, this value is many times smaller than the laser beam size and, second, much greater than the GST thickness. Therefore, we consider the lateral heat flow negligible in our experiment, and the heat conductance is effectively one-dimensional, proceeding normal to the film surface.

For all the investigated samples, the observed in Fig. 5 tendency of TFC lowering with increased number of laser pulses retains. Fig. 6 shows TFC values for the studied samples. As can be seen from the figure, the TFC value depends strongly on the nature of substrate as well as the GST film thickness. The shaded area on the plots denotes the range of pulse numbers which provoke pale spots formation only, without signs of crystallization. In this case, the TFC is related to the threshold of pale spots formation. Nevertheless, it is clear from Fig. 6 that both pale spots formation threshold (the data in the shaded area) and crystallization threshold belong to the same experimental curve. It implies that the mechanisms of formation of pale spots and crystalline areas are inherently the same, and only the number of laser pulses defines the final result of laser irradiation. Apparent threshold number of laser pulses, which separates formation of pale spots from crystalline areas, in its turn, is

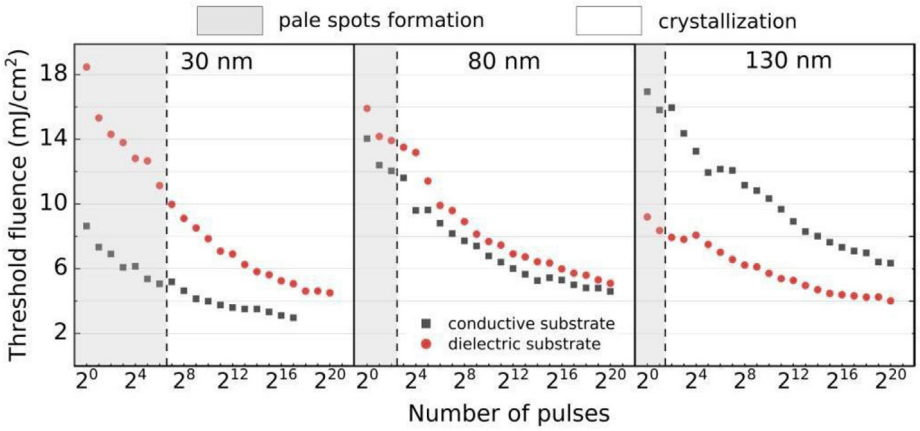

Fig. 6. Dependences of threshold fluence of modification on number of pulses for various film thicknesses and substrate types.

independent of the substrate type but at the same time sensitive to the film thickness.

4. Discussion

Our results indicate that the formation of bright crystalline spots on the GST film takes many ultra-short laser pulses. The pale spots formed under a small number of laser pulses do not fall into this category, and we postpone their discussion to the final stage of this section. The necessity of multi-pulsed excitation suggests to investigate the evolution of recorded marks with respect to the pulse number (that is, left-to-right in Fig. 2). Two distinct regimes of crystalline marks formation are evident in Fig. 2. The marks formed under low energy excitation (100 nJ) exhibit growth from the centre of the laser beam with increasing number of pulses. The second regime of growth, corresponding to higher pulse energies (e.g., 200 nJ), is more complex. Initially, a pale spot develops, and only after a considerable number of laser pulses a crystalline ring forms at the edge of the modified area. Under subsequent pulses, the crystalline ring grows both outward, leading to increase of the recorded mark size, and inward, eventually filling the recorded mark with crystalline material.

4.1. Threshold fluence for crystallization

Despite the difference in the growth regime between the crystalline marks recorded using different pulse energies, we reiterate here, that the TFC value does not depend on the pulse energy. Based on this observation, which we have concluded above, the increase of recorded marks area is controlled by the local value of laser fluence. Here, we reformulate this conclusion. Being controlled by a local laser fluence, the very crystallization process at the outer edge of recorded marks consists of *local* emerging of crystalline phase. In other words, the phase state of surrounding material does not impact upon this process. Two experimental observations are available describing this type of crystallization. Firstly, the multi-pulsed excitation is vital for this process (Fig. 2). Secondly, the higher the local laser fluence the lower number of laser pulses is necessary for crystallization (Fig. 5). The conclusion to be drawn from the first one is that *each* laser pulse, even the one producing no observable changes, provides a finite impact on the material, and this impact is accumulated somehow between pulses. Second observation, in its turn, suggests that this finite impact is proportional to the local laser fluence. As stated above, the characteristic thermal diffusion length for 200 kHz repetition rate far exceeds the film thickness. Thus, the accumulative finite impact is not thermal.

From the other side, the essence of crystallization comprises nucleation and growth processes. The nature of the nucleation process is transient [26] in a sense that a new value of nucleation rate, corresponding to the suddenly elevated temperature of the material, is established only after the time lag, which is often called *incubation time* in literature. Therefore, we believe that initial laser pulses, which precede the formation of detectable amounts of crystalline phase, could be perceived as incubation pulses. In Refs. [27], on the basis of the static tester experiments authors concluded that there is a pronounced threshold time for the crystallization under CW laser irradiation - shorter exposure does not induce crystallization. Although being obtained with longer pulses of a CW laser, their results are inherently the same as ours — except that in our experiment the time axis is discrete, and we measure the duration of the initial incubation stage in the number of laser pulses. This initial stage of crystallization leads to formation of stable distribution of nuclei. Once a sufficient number of crystallization sites becomes available, the growth process gets involved effectively producing macroscopically crystalline areas. Thus, we can expect in our case, that the finite impact of each pulse is none other than nucleation centers. Nuclei are accumulated between pulses, and upon reaching a sufficient number of them, the crystallization by means of their growth is initiated. For the GST, the increase of incubation time for lower temperatures is shown experimentally [28]. Therefore, the weaker laser fluence impacts the material, the longer is the incubation stage and the more laser pulses are necessary to produce the stable nuclei distribution. This hypothesis could be used to explain both the dependence of TFC on the number of pulses (Fig. 5) and the fact that crystalline marks are formed only after a considerable number of pulses (Fig. 6).

The described above mechanism provides the degree of understanding the process of local crystalline phase formation to proceed further to the discussion of the substrate type influence on this process. In Fig. 6, the results of threshold fluence determination for various GST film thicknesses on different substrates are presented. Let us start from the 130 nm film. This value is larger than the light penetration depth. It is evident from Fig. 6 that the value of TFC is lower for the dielectric substrate, suggesting that the crystallization is facilitated in this case. Poor thermal conductivity of the dielectric material hinders the heat removal from the film into the substrate and therefore higher temperatures could be achieved for a prolonged time period in response to a laser pulse promoting crystallization. In contrast, the 30 nm film shows the opposite behavior, with the crystallization being favourable on the

conductive substrate. In this case, the film thickness is less than the light penetration depth and a considerable amount of light reaches the substrate. Depending on the substrate type, this light is either transmitted to the silicon wafer through the oxide film or reflected and absorbed by the metallic one. In the first case, the energy carried by the portion of light reaching the substrate becomes removed from the GST film. Metallic layer, conversely, returns the light to the GST film providing an additional source of heat. Thus, for the thin 30 nm film the conductive substrate becomes favourable for crystallization. We can conclude therefore that both types of substrate could either facilitate or inhibit the crystallization, depending on the film thickness. For the 80 nm film, the data obtained for different substrates are closer to each other which suggests that in this intermediate regime facilitation/inhibition effects tend to compensate each other.

4.2. Crystalline rings formation

Now, we are getting back to the second aforementioned regime of modified areas formation, that is, the crystalline rings. Growth of crystalline rings proceeds twofold: both outward and inward (Fig. 2). Taking into account higher pulse energy, Gaussian distribution of laser fluence in the beam and our notion of TFC, both directions of crystalline rings growth can be explained. At the periphery of the laser beam, where fluence has reached the required TFC level, crystallization of the outer part of the mark occurs, as discussed above. However, closer to the beam centre the fluence turns out to be so high, that it reaches the threshold level of material melting. Thus, we believe that inward growth of crystalline rings is caused by local melting of amorphous film and its further quenching.

To melt the material, first, the energy sufficient for heating it from initial temperature T_0 up to the melting point T_m must be furnished and, second, heat of fusion ΔH_m has to be supplied. In total, the sum evaluates to the surface density of energy (which is the same as the fluence) necessary to melt the material layer of thickness h. Here ρ and c denote density and specific heat of the material, respectively. The published data [21,25,29,30] regarding corresponding properties of GST allows estimating F_m for the 30 nm film as 4.2 mJ/cm^2. This value is indeed within the range of laser fluences utilized in this study (for pulse energies above 100 nJ), which gives reasons to anticipate the presence of melting in our experiment.

$$F_m = hpc(T_m - T_0) + hp\Delta H_m \quad (1)$$

However, the question remains: why does the mark not crystallize completely and instead a ring is formed? It is widely accepted that the microstructure formation during solidification is to a great extent controlled by the cooling rate. In Ref. [31] the transmission electron microscopy (TEM) images of laser-induced crystallization of GST are given together with finite element modeling of the heating effect of laser pulses. It has been concluded that the morphology of grains is controlled by the temperature gradient in the film. Increase of the gradient with higher laser fluences led to formation of larger columnar grains. The increase of grain size proportional to laser fluence is also reported in Ref. [32,33]. Authors of [34] performed comparison of the modeling results with AFM images of GST films and proposed the time-temperature diagram that predicts transformation from fully to partially crystallized structure and eventually to glassy state with increase of cooling rate. Ultimately, solidification of a melt could indeed produce two different phases: crystalline and glassy.

Therefore, the formation of crystalline rings in our experiment could be explained as follows. After a laser pulse, the molten region forms. The heat is constantly removed from the material into the substrate, and eventually it will start to solidify. Diameter of the molten region will gradually decrease. The lesser the volume of melt is, the lesser the amount of heat that must be removed to provide the solidification, which effectively speeds up the solidification process. This positive feedback makes us conclude that the speed of the melt-solid interface constantly increases during cooling, reaching its maximum at the very centre of the melted region. Initially, the interface movement is slow enough to provide the crystallization process with sufficient time for its completion. Thus, crystalline fraction forms following the solid-melt interface. Eventually, however, the rate of its movement will exceed the rate of the crystallization process leading to formation of the glassy phase in the middle of the modified region. Thus, a bright crystalline ring with darker glassy inner area forms.

Shrinkage of the central glassy area after subsequent pulses could as well be described within the outlined physical picture. After a bright crystalline ring is formed, its increased reflectivity will decrease the amount of absorbed light during subsequent pulses. So, subsequent pulses can affect only on the glassy centre, again starting the melt-quenching process. Therefore, the diameter of the melted region decreases after each subsequent pulse.

Further insights into the mechanisms of crystalline rings formation are provided by more detailed AFM measurements. In Fig. 7, individual grains of polycrystalline structure are visible. Three distinct regions are indicated in Fig. 7 on the basis of differences in grain morphology. Region I, the inner dark area, is glassy and exhibits a smooth featureless morphology. Its surface is about 1 nm above the surrounding crystalline phase, which is in line with the density change of GST upon crystallization. Region II is composed of large individual grains, forming the recognizable polycrystalline pattern with decreasing average grain size from centre to periphery. Relatively high roughness of the region III (1.11 nm, in contrast to 0.19 nm and 0.27 nm for regions I and II, respectively) suggests to consider it composed of a great number of very fine grains.

The decrease in the grains concentration, depicted in Fig. 7, explains the mechanism of inhibition of crystallization process with increased cooling speed. Concentration of grains is related here to the rate of nucleation near the solid-melt interface. Decrease of grains concentration toward the centre of modified areas indicates that it is the nucleation process what becomes suppressed by an increased cooling speed.

Fig. 7 shows that the grains are aligned with respect to the elliptical shape of the recorded mark. We believe this form of grains is provided by different widths of the intensity distribution of the laser beam along two axes (Fig. 1(b)). The larger width leads to the lower temperature gradient and consequently slower movement of the solid-melt interface. Apparently, the growth of individual grains

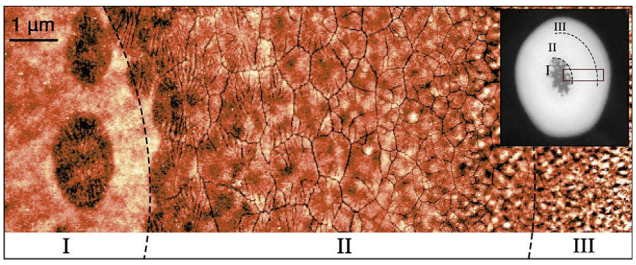

Fig. 7. Tapping-mode AFM image of polycrystalline structure of a ring-shaped mark. A decreasing concentration of crystalline grains in the direction from the periphery to the spot centre is readily observed. The optical image of the spot is shown in the inset, image size is 50 × 50 μm; white frame marks the place of AFM scan (spot formation parameters: 200 nJ, × 2^9 pulses, 30 nm-thick GST layer on the conductive substrate).

could be thus enhanced along the major axis of the laser beam ellipse.

4.3. Pale spots formation

Finally, the nature of pale spots preceding the formation of crystalline rings should be discussed. In Fig. 8, an AFM image of a pale spot (at the top) is overlaid onto an AFM image of a crystalline ring (at the bottom), which was formed under the same energy of laser pulses but a greater number of them. The size of the pale spot is practically equal with the size of the region II of the crystalline ring (Fig. 7). Furthermore, the morphology of the pale spot is very close to that of the region I according to both AFM (Fig. 8) and optical microscopy (Fig. 2). Furthermore, Raman spectroscopy did not allow to detect any differences between pale spots and initial amorphous material. So we consider that the pale spots are formed by the same melt-quenching process as the one that leads to the crystalline rings formation.

There is a pulse number threshold below which the crystalline phase cannot be formed (shaded area in Fig. 6). Fig. 2 shows that for 30 nm film the required threshold lies in the range from 64 to 128 pulses. That threshold appears to be independent of the pulse energy (Fig. 2) and substrate conductivity within the same film thickness (Fig. 6). For thicker films (80 and 130 nm) the fewer number of laser pulses is sufficient for the crystallization (Fig. 6). Thus, for 80-nm film crystallization starts after 8 pulses, and 130-nm film crystallizes after 4 pulses. However, the melt-quenching regime is initiated with larger pulse energies for thicker films which is in line with (1). The minimum energies required for melting for 30, 80, and 130 nm films are, respectively, 150, 350 and 500 nJ. With a similar trend it seems possible to select such ratio “film thickness/pulse energy” to initiate the crystallization process with a single laser pulse.

These observations can be explained if we consider the threshold number of pulses as a discrete incubation time (as described above). In our case, it turns out that the duration of the incubation period does not depend on the laser parameters (Fig. 6), but at the same time rises with reduction of the film thickness. From the literature it is known that atomic mobility decreases with decreasing film thickness [35,36]. Consequently, the stable nuclei may take longer to form in thinner films. It can be assumed that the experimentally observed absence of crystallization for amorphous ultrathin films of several nanometers thickness for a number of telluride based compositions of PCM materials is associated with this phenomenon also [37].

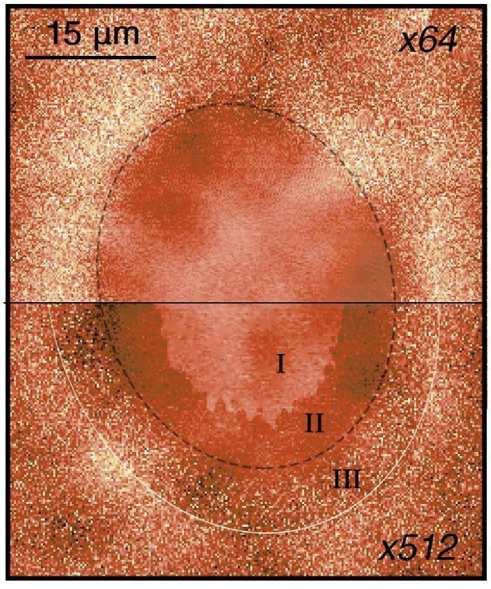

Fig. 8. On the nature of pale spots (spots were formed by 64 and 512 pulses with energy 250 nJ).

It should also be noted that the incubation period does not depend on the regime of recorded marks formation: both outward growing spots (100 nJ) and crystalline rings emerge at the same number of pulse repetitions for a given film thickness. And this is why we observe the smooth transition from pale spots formation to crystalline rings formation threshold in Fig. 6. Recalling that the TFC value does not depend on the regime of marks formation and taking into account the results presented in Fig. 8 we could make the following conclusion. The local formation of crystalline phase, which leads to outward growth of recorded marks, and the crystallization from the melt, which controls the formation of crystalline rings, are triggered simultaneously. We assume that both growth regimes start when the crystalline phase has been formed in the vicinity of the border between zones II and III in Fig. 8 due to multiple laser pulses under the melting threshold. Under subsequent laser pulses, growth of the crystalline ring proceeds both outward - due to local crystalline phase formation in the zone III, and inward - by the melt-quenching process in the zone II.

5. Conclusion

Two distinct regimes of crystalline marks formation on the surface of GST thin films are attributed to the Gaussian distribution of the intensity in the laser beam. It is shown that there are two ways of crystalline phase formation in GST under femtosecond pulses excitation.

At the moderate value of laser fluence, crystalline fraction forms inside the solid amorphous phase. This process is apparently two-stage. It takes a substantial number of laser pulses to achieve the formation of the crystalline phase and during this initial stage the incubation of crystalline nuclei proceeds. Subsequent pulses provide growth of nuclei, leading to formation of macroscopically crystalline areas. The lower value of laser fluence hits the sample surface, the more pulses are necessary to induce this process. This way of crystallization leads to formation of fine-grained polycrystalline material.

The second way of crystallization proceeds at higher levels of the laser fluence, closer to the beam centre. The film material melts and subsequent solidification of the melt provides conditions for large crystalline grains formation at the edge of the molten region. As the edge moves towards the centre during solidification, its velocity increases, leading to inhibition of the nucleation process. Therefore, larger grains are produced closer to the beam centre, and eventually no new nuclei can be formed due to high cooling velocity leading to formation of a glassy phase in the centre of marks.

Metallic and oxide substrates are shown to impact the laser-induced crystallization of GST film differently, depending on the film thickness. If the GST film is thicker than the light penetration depth, crystallization proceeds easily on the dielectric substrate due to the lack of thermal conductivity and consequent heat accumulation. For the film thinner than the penetration depth crystallization is favourable on the conductive substrate. In this case, the laser beam is reflected from the film-substrate interface and returned to the film, enhancing the heating effect.

Author’s contribution

The corresponding author, Tatyana Kunkel, is responsible for ensuring that the descriptions are accurate and agreed by all

authors.

CRediT authorship contribution statement

Tatyana Kunkel: Conceptualization, Methodology, Investigation, Data curation, Writing - original draft. **Yuri Vorobyov:** Conceptualization, Methodology, Investigation, Writing - original draft. **Mikhail Smayev:** Methodology, Investigation, Writing - original draft. **Petr Lazarenko:** Resources, Methodology, Investigation, Writing - original draft. **Vladimir Veretennikov:** Data curation, Writing - review & editing. **Vladimir Sigaev:** Supervision, Methodology. **Sergey Kozyukhin:** Conceptualization, Methodology, Supervision, Project administration, Writing - original draft, Funding acquisition.

Declaration of competing interest

The authors declare that they have no known competing financial interests or personal relationships that could have appeared to influence the work reported in this paper.

Acknowledgements

This work was supported by the RFBR (project 20-03-00379) and the Russian Federation President's grant (MK-727.2020.3). The sample preparation was performed using equipment of Core facilities centre "MEMS and electronic components" and "STI Sensory" of MIET. Optical and AFM studies were performed using equipment of the Regional Centre for Probe Microscopy of RSREU.

References

[1] N. Yamada, E. Ohno, K. Nishiuchi, N. Akahira, M. Takao, Rapid-phase transitions of GeTe-Sb_2Te_3 pseudobinary amorphous thin films for an optical disk memory, J. Appl. Phys. 69 (1991) 2849–2856, https://doi.org/10.1063/1.348620.

[2] H. Seo, T.-H. Jeong, J.-W. Park, C. Yeon, S.-J. Kim, S.-Y. Kim, Investigation of crystallization behavior of sputter-deposited nitrogen-doped amorphous $Ge_2Sb_2Te_5$ thin films, Jpn. J. Appl. Phys. 39 (2000) 745–751.

[3] G. Ruitenberg, A.K. Petford-Long, R.C. Doole, Determination of the isothermal nucleation and growth parameters for the crystallization of thin $Ge_2Sb_2Te_5$ films, J. Appl. Phys. 92 (2002) 3116–3123, https://doi.org/10.1063/1.1503166.

[4] S. Senkader, C.D. Wright, Models for phase-change of $Ge_2Sb_2Te_5$ in optical and electrical memory devices, J. Appl. Phys. 95 (2004) 504–511, https://doi.org/10.1063/1.1633984.

[5] I.V. Karpov, M. Mitra, D. Kau, G. Spadini, Y.A. Kryukov, V.G. Karpov, Evidence of field induced nucleation in phase change memory, Appl. Phys. Lett. 92 (2008), 173501, https://doi.org/10.1063/1.2917583.

[6] V.G. Karpov, Y.A. Kryukov, M. Mitra, I.V. Karpov, Crystal nucleation in glasses of phase change memory, J. Appl. Phys. 104 (2008), 054507, https://doi.org/10.1063/1.2973686.

[7] J. Orava, A.L. Greer, Classical-nucleation-theory analysis of priming in chalcogenide phase-change memory, Acta Mater. 139 (2017) 226–235, https://doi.org/10.1016/j.actamat.2017.08.013.

[8] T.H. Lee, S.R. Elliott, The relation between chemical bonding and ultrafast crystal growth, Adv. Mater. 29 (2017), 1700814, https://doi.org/10.1002/adma.201700814.

[9] W. Zhang, R. Mazzarello, M. Wuttig, E. Ma, Designing crystallization in phase-change materials for universal memory and neuro-inspired computing, Nat. Rev. Mater 4 (2019) 150–168, https://doi.org/10.1038/s41578-018-0076-x.

[10] G.-F. Zhou, B.A.J. Jacobs, High performance media for phase change optical recording, Jpn. J. Appl. Phys. 38 (1999) 1625–1628.

[11] S.-H. Lee, Y. Jung, R. Agarwal, Size-dependent surface-induced heterogeneous nucleation driven phase-change in $Ge_2Sb_2Te_5$ nanowires, Nano Lett. 8 (2008) 3303–3309, https://doi.org/10.1021/nl801698h.

[12] S. Raoux, H.-Y. Cheng, J.L. Jordan-Sweet, B. Muñoz, M. Hitzbleck, Influence of interfaces and doping on the crystallization temperature of Ge–Sb, Appl. Phys. Lett. 94 (2009), 183114, https://doi.org/10.1063/1.3133344.

[13] W.J. Wang, L.P. Shi, R. Zhao, K.G. Lim, H.K. Lee, T.C. Chong, Y.H. Wu, Fast phase transitions induced by picosecond electrical pulses on phase change memory cells, Appl. Phys. Lett. 93 (2008), 043121, https://doi.org/10.1063/1.2963196.

[14] M. Friesel, Bulk phase transitions of cesium hydrogen sulphate initiated by surface processes, grinding or external pressure, Solid State Ionics 35 (1989) 91–98, https://doi.org/10.1016/0167-2738(89)90017-9.

[15] A. Zakery, S.R. Elliott, Optical Nonlinearities in Chalcogenide Glasses and Their Applications, Springer, 2007.

[16] C. Yuan, R.S. Smith, B.D. Kay, Surface and bulk crystallization of amorphous solid water films: confirmation of "top-down" crystallization, Surf. Sci. 652 (2016) 350–354, https://doi.org/10.1016/j.susc.2015.12.037.

[17] P.I. Lazarenko, Y.V. Vorobyov, M.E. Fedyanina, A.A. Sherchenkov, S.A. Kozyukhin, A.O. Yakubov, A.V. Kukin, Y.S. Sybina, I.V. Sagunova, Peculiarities of estimating the optical band gap of thin films of phase change memory materials, Inorg. Mater. Appl. Res 11 (2020) 330–337, https://doi.org/10.1134/S2075113320020227.

[18] G. Zhang, D. Gu, X. Jiang, Q. Chen, F. Gan, Crystallization of amorphous $Ge_2Sb_2Te_5$ films induced by a single femtosecond laser pulse, Solid State Commun. 133 (2005) 209–212, https://doi.org/10.1016/j.ssc.2004.11.013.

[19] Y. Liu, M.M. Aziz, A. Shalini, C.D. Wright, R.J. Hicken, Crystallization of $Ge_2Sb_2Te_5$ films by amplified femtosecond optical pulses, J. Appl. Phys. 112 (2012), 123526, https://doi.org/10.1063/1.4770359.

[20] J. Siegel, W. Gawelda, D. Puerto, C. Dorronsoro, J. Solis, C.N. Afonso, J.C.G. de Sande, R. Bez, A. Pirovano, C. Wiemer, Amorphization dynamics of $Ge_2Sb_2Te_5$ films upon nano- and femtosecond laser pulse irradiation, J. Appl. Phys. 103 (2008), 023516, https://doi.org/10.1063/1.2836788.

[21] W.K. Njoroge, H.-W. Wöltgens, M. Wuttig, Density changes upon crystallization of $Ge_2Sb_{2.04}Te_{4.74}$ films, J. Vac. Sci. Technol. 20 (2002) 230–233, https://doi.org/10.1116/1.1430249.

[22] T. Nonaka, G. Ohbayashi, Y. Toriumi, Y. Mori, H. Hashimoto, Crystal structure of GeTe and $Ge_2Sb_2Te_5$ meta-stable phase, Thin Solid Films 370 (2000) 258–261, https://doi.org/10.1016/S0040-6090(99)01090-1.

[23] S. Kozyukhin, P. Lazarenko, Y. Vorobyov, A. Baranchikov, V. Glukhenkaya, M. Smayev, A. Sherchenkov, Y. Sybina, A. Polohin, V. Sigaev, Laser-induced modification and formation of periodic surface structures (ripples) of amorphous GST225 phase change materials, Optic Laser. Technol. 113 (2019) 87–94, https://doi.org/10.1016/j.optlastec.2018.12.017.

[24] S. Kozyukhin, Y. Vorobyov, A. Sherchenkov, A. Babich, N. Vishnyakov, O. Boytsova, Isothermal crystallization of $Ge_2Sb_2Te_5$ amorphous thin films and estimation of information reliability of PCM cells, Phys. Status Solidi 213 (2016) 1831–1838, https://doi.org/10.1002/pssa.201532930.

[25] J.L. Battaglia, A. Kusiak, V. Schick, A. Cappella, C. Wiemer, M. Longo, E. Varesi, Thermal characterization of the SiO_2-$Ge_2Sb_2Te_5$ interface from room temperature up to 400°C, J. Appl. Phys. 107 (2007), 044314, https://doi.org/10.1063/1.3284084.

[26] K.F. Kelton, Crystal nucleation in liquids and glasses, Solid State Phys. 45 (1991) 75–177, https://doi.org/10.1016/S0081-1947(08)60144-7.

[27] J.H. Coombs, A.P.J.M. Jongenelis, W. van Es-Spiekman, B.A.J. Jacobs, Laser-induced crystallization phenomena in GeTe-based alloys. I. Characterization of nucleation and growth, J. Appl. Phys. 78 (1995) 4906–4917, https://doi.org/10.1063/1.359779.

[28] V. Weidenhof, I. Friedrich, S. Ziegler, M. Wuttig, Laser induced crystallization of amorphous $Ge_2Sb_2Te_5$ films, J. Appl. Phys. 89 (2001) 3168–3176, https://doi.org/10.1063/1.1351868.

[29] J. Kalb, F. Spaepen, T.P. Leervad Pedersen, M. Wuttig, Viscosity and elastic constants of thin films of amorphous Te alloys used for optical data storage, J. Appl. Phys. 94 (2003) 4908, https://doi.org/10.1063/1.1610775.

[30] C. Cabral, K.N. Chen, L. Krusin-Elbaum, V. Deline, Irreversible modification of $Ge_2Sb_2Te_5$ phase change material by nanometer-thin Ti adhesion layers in a device-compatible stack, Appl. Phys. Lett. 90 (2007), 051908, https://doi.org/10.1063/1.2450656.

[31] Z. Zhu, F.R. Liu, J.F. Yang, Z.K. Fan, F. Liu, N.X. Sun, A cross sectional study on the crystallization of amorphous $Ge_2Sb_2Te_5$ films induced by a single-pulse ultraviolet laser, Optic Laser. Technol. 81 (2016) 100–106, https://doi.org/10.1016/j.optlastec.2015.10.010.

[32] X. Sun, M. Ehrhardt, A. Lotnyk, P. Lorenz, E. Thelander, J.W. Gerlach, T. Smausz, U. Decker, B. Rauschenbach, Crystallization of $Ge_2Sb_2Te_5$ thin films by nano- and femtosecond single laser pulse irradiation, Sci. Rep. 6 (2016) 28246, https://doi.org/10.1038/srep28246.

[33] J.C. Guo, F.R. Liu, W.Q. Li, T. Fan, Y.Z. Zhang, N.X. Sun, F. Liu, Microstructure evolution of the crystallization of amorphous $Ge_2Sb_2Te_5$ thin films induced by single picosecond pulsed laser, J. Non-Cryst. Solids 498 (2018) 1–7, https://doi.org/10.1016/j.jnoncrysol.2018.06.014.

[34] F.R. Liu, N. Bai, J.J. Zhao, X.X. Han, W.P. Zhou, X. Lin, N.X. Sun, An explanation of the crystallization of amorphous $Ge_2Sb_2Te_5$ films induced by a short Gaussian laser pulse, Appl. Phys. Lett. 103 (2013), 051905, https://doi.org/10.1063/1.4817251.

[35] H. Schönherr, C.W. Frank, Ultrathin films of poly(ethylene oxides) on oxidized silicon. 2. In situ study of crystallization and melting by hot stage AFM, Macromolecules 36 (2003) 1199–1208, https://doi.org/10.1021/ma020686a.

[36] S. Napolitano, M. Wübbenhorst, Slowing down of the crystallization kinetics in ultrathin polymer films: a size or an interface effect? Macromolecules 39 (2006) 5967–5970, https://doi.org/10.1021/ma061304u.

[37] S. Raoux, J.L. Jordan-Sweet, A.J. Kellock, Crystallization properties of ultrathin phase change films, J. Appl. Phys. 103 (2008), 114310, https://doi.org/10.1063/1.2938076.